Rheol Acta (2005) 44: 379–395
DOI 10.1007/s00397-004-0420-5

ORIGINAL CONTRIBUTION

Xiao-Dong Pan

Impact of reinforcing filler on the dynamic moduli of elastomer compounds under shear deformation in relation to wet sliding friction

Received: 12 April 2004
Accepted: 30 September 2004
Published online: 2 December 2004

X.-D. Pan
Bridgestone/Firestone Research, LLC,
1200 Firestone Parkway,
Akron, OH 44317-0001, USA
E-mail: panxiaodong@bfusa.com
Tel.: +1-330-3797339
Fax: +1-330-3797530

Abstract In pursuit of a better understanding of the relationship between wet sliding friction and bulk viscoelastic properties of elastomer compounds, especially the contribution from different reinforcing fillers, the linear thermorheological behavior, the nonlinear dynamic moduli under shear deformation (for strain up to about 140%), and the wet sliding friction have been characterized in detail for crosslinked compounds of low-*cis* polybutadiene filled with different reinforcing fillers including carbon black, graphitized carbon black, and precipitated silica. We examine the scenario of possible extra energy dissipation via higher harmonic excitation in rubber compounds coupled with dynamic deformation consisting of components at many frequencies during sliding of rubber on a rough surface. While no straightforward explanation is identified relating the observed difference in wet sliding friction arising from different fillers to the bulk viscoelastic properties, some unexpected viscoelastic features arising from the compounds are observed.

Keywords Sliding friction · Elastomer · Filler · Nonlinear dynamic moduli · Higher harmonic excitation

Introduction

The wet sliding friction of reinforced rubber compounds affects the safety of the driving public. Before the emergence of elastohydrodynamic lubrication at high driving speed, the material properties of the tread rubber on a pneumatic tire play a significant role in determining the friction level. Here we deal with the situation in which the rubber compound is the only variant in the tribo-system consisting of the rubber compound, the (rough) road surface, and the water in-between. For the purpose of rational material design it is obviously desirable to know exactly what material properties affect the friction level. At present this issue is far from being resolved [14, 39].

It has been generally agreed that for wet sliding friction of rubber in the boundary lubrication regime, tear of rubber and adhesion between rubber and the road surface still contribute to the overall friction present [14, 39]. However, the friction level is dominated by the hysteretic loss in rubber because of its dynamic deformation at high frequencies induced by the multi-scale asperities on the road surface. Although a causal quantification of contribution to friction from tear or adhesion is still absent, the outstanding friction behavior of butyl rubber has been explained with a-posteriori counting of material wear loss [42], in addition to other considerations of its unique viscoelastic behavior [13, 15].

It has long been disputed whether or not the hysteretic friction is mainly influenced by the smaller asperities on the road surface [26]. The recent argument [30] favoring the smaller asperities is of concern, because it neglects the difference in volume of material "excited" by the asperities at different length scale. It has been suggested that if the ratio between the amplitude and

wavelength is scale-independent then surface roughness at different length scale contributes equally to the friction force [33].

The master curve approach pioneered by Grosch [13] has been widely accepted and has been regarded as direct proof of the viscoelastic nature of rubber friction (on both smooth and rough surfaces). For elastomers exhibiting no strain-induced crystallization, the coefficient of friction μ depends on the reduced variable $a_T(T)v$ but is less sensitive to (non-trivial) pressure or load on a rough surface [14]. Here T is the test temperature, $a_T(T)$ is the William–Landel–Ferry (WLF) time–temperature shift factor, and v is the sliding speed.

In the last decade or so, precipitated silica used with a sulfur-containing silane is rapidly gaining ground in replacing conventional carbon black as the reinforcing filler of choice for preparing the so-called ''green'' tire. This can lead to reduced tire rolling loss with simultaneous improvement in wet sliding friction. However, the effect of silica on wet sliding friction has not been well explained on the basis of viscoelastic criteria. A number of intuitive (non-viscoelastic) assumptions have been proposed [7, 46]. Further complicating the puzzle, tire testing reveals that the dry sliding friction for a silica-filled rubber compound is no better than that for a carbon black-filled rubber compound. Complication may arise from the severe frictional heating during dry sliding.

For unlubricated sliding of ductile metals [37, 38], the grain-boundary in the material acts as a marker revealing the large *plastic* strains and strain gradients adjacent to the sliding interface. Depending on the system and the sliding conditions, the deformation can extend from a few micrometers to hundreds of micrometers into the bulk. The shear displacement (or strain) reduces exponentially with the distance from the surface. In one case of copper sliding against stainless steel, after sliding 12 m at 1 cm s^{-1}, the shear strain at the surface is estimated to exceed 1000% whereas the surface strain rate is of the order of 10^3 s^{-1}.

In contrast, there is no inherent marker in a rubber compound. In a recent theoretical investigation of rubber friction [33], the strains involved when sliding on a road surface are assumed to be of the order of 100%. On the other hand, actual testing of ''veneered'' tires [6] indicate that the wet sliding friction is determined by the properties of the outer layer of tread material no more than 0.2 mm thick. Current theories of rubber friction [19, 33] have not addressed such veneer effect and the suggestion of sub-surface regions of maximum hysteresis loss based on a quasi-elastic considerations [12, 47].

It is therefore reasonable to contemplate the possibility of resolving the mystery surrounding the role of silica in wet sliding friction by examining the viscoelastic response of a rubber compound under large deformation. Practically the only material quantities employed in discussing sliding friction of rubber have been the dynamic moduli ($G^* = G' + iG''$), mostly measured under an imposed sinusoidal shear strain $\gamma = \gamma_0 \sin(2\pi ft)$. Here $G'$is the storage modulus, G'' is the loss modulus, γ_0 is the strain amplitude, and f is the oscillation frequency. However, so far there have appeared only a few scattered reports of G^* tested to large γ_0 (up to $\sim$100%) for vulcanized rubber compounds [16, 45]. Most importantly, excitation of odd higher harmonics in the stress response are expected for nonlinear viscoelastic materials [5].

Filled rubber compounds typically exhibit a distinctively nonlinear dependence of G^* on γ_0. The reduction of G' with γ_0 has been conventionally termed the Payne effect in the rubber industry. The existence of a filler network in the compound is considered by many to be responsible for the Payne effect [16, 18]. It has been pointed out that for γ_0 between 0.1 and 1% where G' markedly changes with γ_0, an undistorted sinusoidal output is still obtained in response to a sinusoidal input [40]. For several unfilled and filled elastomer compounds at γ_0 between 0.1 and 20%, analysis of the response signal with a digital oscilloscope with the fast Fourier transform (FFT) capabilities reveals only very small higher harmonic content, even in the presence of a static strain at 10% [3]. However, systematic examination of the extent of higher harmonic excitation at large deformation has yet to appear for vulcanized filled rubber compounds.

For Green–Rivlin solids it has well been recognized that for a single frequency strain input, energy can only be dissipated at the frequency of excitation [8]. However, the irregular multi-scale asperities on a road surface obviously cause dynamic deformation consisting of components at many frequencies. If the extent of higher harmonic excitation in rubber compounds were significant, the overall friction present would include the extra energy dissipation at the excited higher harmonics picked up by the road surface. Such extra energy dissipation would have been lost from the simple consideration of the apparent G'' or loss tangent $\tan\delta$ as reported directly by the testing instrument even if tested at large γ_0.

Such a scenario becomes more appealing considering the following situation. In the absence of sliding, tread material is deformed under the vehicle weight. Therefore the dynamic deformation of the rubber sliding over surface asperities will be superposed on to the static deformation due to the vehicle weight. For non-Newtonian fluids undergoing a steady shearing motion in the same direction as a superposed finite-amplitude oscillation, both even and odd harmonic shear stresses are expected to be excited in the fluid [44]. It has been reported in one study that the amplitude of the second harmonic can be 40% of that of the basic frequency while the amplitude of the third harmonic is less than 10% of that of the basic frequency signal [34].

In this investigation, we examine the effects of different reinforcing fillers (carbon black, graphitized carbon black, and precipitated silica) on G^* and the wet sliding friction of rubber compounds. To avoid further complication from polymer transition, a low-*cis* polybutadiene rubber (BR) of low thermal glass transition temperature T_g is chosen as the matrix polymer. The linear thermorheological behavior is characterized. The stress response of the *rubbery* compounds at 0°C or at room temperature (RT) is examined in detail under an imposed sinusoidal shear strain in the parallel plate geometry. The range of testing includes γ_0 up to ~140% and f at 0.1, 1, or 10 Hz. Fourier transform is performed on the stress response to reveal the extent of higher harmonic excitation. The effects from the existence of a static strain γ_m superposed in parallel are also investigated. Wet sliding friction is tested with a portable British Pendulum Skid Tester (BPST) at RT or between 0 and 40°C.

For model suspensions of monodisperse spherical particles in liquids of small molecular weight, explicit consideration of interparticle colloidal forces has entered into the quantitative interpretation of suspension rheology [41, 43]. This is obviously difficult for the compounds under study here. Not only can an individual filler particle entity consist of a number of more or less spherical primary particles randomly fused together, but also filler–polymer interactions generate heterogeneity in the molecular mobility of the polymer phase. However, efforts have been made to establish "micro-mechanical" models of nonlinear viscoelasticity based on fractal approaches of filler networking (percolation or cluster-cluster aggregation) [16, 18]. It is still insufficient to account for the markedly enhanced energy dissipation in filled rubber with current micro-mechanical models.

There have been many discussions on the rheological characterization of the nonlinear viscoelastic response of various polymeric materials under oscillatory deformation [9, 25, 44]. Higher harmonic excitation has been examined for pure polymers [5, 9, 48], polymer solutions [35, 36], crosslinked filled elastomer compounds at small strain ($\gamma_0 \leq 6.0\%$) [8], and unvulcanized gum or carbon black-filled rubber compounds in a more complicated geometry on a "Rubber Process Analyzer" [22, 23].

Experimental

A commercial low-*cis* BR (Taktene 4510 from Bayer Polymers) was employed as the matrix polymer. Its midpoint T_g according to differential scanning calorimetry (DSC) characterization at a heating rate of 10 °C min^{-1} was −90.4°C. The nuclear magnetic resonance (NMR) test revealed 37.5% (by weight) *cis*-1,4 content, 51.9% *trans*-1,4 content, and 10.6% 1,2 content for this BR. The gel permeation chromatography (GPC) test indicated a weight-average molecular weight of 198.8×10^3 g mol^{-1} and a polydispersity index of 1.80.

Four different reinforcing fillers were involved in this study: three grades of carbon black and one type of silica. The carbon black was of grade N299 or N339 according to the ASTM designation. The graphitized carbon black N299g was prepared by heating N299 in nitrogen at 2700°C for about 1 h. Graphitization removes all surface functional groups and the highly energetic sites for physical adsorption of polymer. However, it results in only moderate change in the gross morphology, surface area, and structure [18, 20, 21]. The silica employed was the amorphous precipitated silica commercially available as Hi-Sil 190G from PPG Industries. The typical primary particle size according to electron microscopy was between 20 and 25 nm for N299, between 26 and 30 nm for N339, and averaged at 17 nm for Hi-Sil 190G. The nitrogen-adsorption surface area (according to the Brunauer–Emmett–Teller equation) was 96, 103, 94.2, and 215 m^2 g^{-1} corresponding to N339, N299, N299g, and Hi-Sil 190G, respectively.

A total of six different compounds were prepared with this BR according to the formula given in Appendix A. The suffixes -G, -C, and -Silica are used to differentiate a gum compound containing no filler, a carbon black-filled compound, and a silica-filled compound, respectively. All filled compounds contained 50 phr (part per hundred rubber, by weight) of single reinforcing filler. The bifunctional, sulfur-containing organosilane Si69, or bis(triethoxysilylpropyl)tetrasulfane, was applied for one of the two silica-filled compounds prepared. Following the common practice for achieving good mixing, compounding was performed with laboratory internal mixers from C.W. Brabender Instruments. Testing samples were cured in appropriate molds heated to 165°C under high pressure for a specified duration depending on the specific compound.

The filler volume fraction was 0% for BR-G, 18.1% for BR-C-N339, 19.4% for both BR-C-N299 and BR-C-N299g, 16.4% for BR-Silica prepared without the coupling agent Si69, and 15.8% for BR-Silica-Si69 prepared in the presence of Si69. The compounds BR-C-N339, BR-Silica, and BR-Silica-Si69 also contained 10 phr of processing oil. A larger amount of sulfur was used to cure BR-Silica to compensate possible adsorption of sulfur on to the silica surface in the absence of Si69.

Related details of testing can be found in earlier reports [30–32]. The tensile strength for the compounds was tested with a Model 4501 Instron Universal Testing Instrument at RT and at a strain rate of 0.167 s^{-1}. The BPST was employed for testing of wet sliding friction without any modification [2, 11; ASTM E303 1993]. The relationship between the instrument reading, British Pendulum (Tester) Number or BPN, and μ is

approximately BPN = 330μ/(3 + μ). A Portland cement concrete patio block provided the sliding surface [32]. The surface asperity profile was scanned with a Surfanalyzer 5000 surface-analysis system from Federal Products with an EPT-1063 high-resolution tip (tip cone angle 90° and tip radius 2.0 μm). The (dynamic) contact pressure between the rubber slider and the concrete surface was revealed with Pressurex pressure-indicating films from Sensor Products. This was performed under dry conditions. The rubber slider slid over the glossy side of the film that was attached at one edge to the concrete surface with a piece of adhesive tape.

The status of filler dispersion in the cured compounds was examined with a light optical microscope (LOM) and an atomic force microscope (AFM). LOM images were obtained from a thin slice of a compound cryogenically cut and in the transmission mode whereas AFM images were acquired in the tapping mode on a freshly exposed surface after a small piece of compound was carefully bisected with a razor blade.

Following the typical procedure, the amount of bound rubber was measured for uncured compounds. It is known that judgment of the intensity of filler–polymer interactions based on bound rubber can only be made under limited controlled conditions [21]. The degree of crosslinking for the cured compounds was also characterized, with the method of equilibrium swelling. A small piece of cured sample was soaked in toluene for more than 72 h. The volume fraction of compound in the network at equilibrium swelling, VR, was calculated.

Dynamic modulus was measured with an advanced rheometric expansion system (ARES) from Rheometric Scientific and an ARES-HT from TA Instruments. The ARES was equipped with an active type force rebalance transducer (with normal force sensing capability, 2 K FRTN1) whereas the ARES-HT was equipped with a high-torque (HT) motor with a passive, spring type standard transducer (10 K STD). During testing of G^*, electrical signals corresponding to torque, strain, and normal force were acquired from the instrument signal panel through a data-acquisition system (DI-700-PGL from DATAQ Instruments). The time delay due to sequential data sampling among different signal channels was corrected by interpolation of the data recorded.

All compounds went through tests of frequency/temperature sweep (for the time–temperature shifting behavior), dynamic time sweep (for the thixotropic behavior), dynamic strain sweep (for the strain-dependency of G^*), and arbitrary waveform (for analyzing the higher harmonic content under imposed sinusoidal shear strain). The torsion rectangular geometry was used for the frequency/temperature sweep test whereas the parallel plate geometry was used for all other tests. For dynamic strain sweep at $\gamma_0 \leq 30\%$ and arbitrary waveform at $\gamma_0 \leq 20\%$, a cylindrical rubber button (approximately 6.0 mm in height and 8.0 mm in diameter) was fixed to two circular end-plates with cyanoacrylate glue and tested with the ARES. For testing at larger γ_0, a rubber disk (approximately 1.9 mm in thickness and 12.7 mm in diameter) was glued to two end plates and tested with the ARES-HT. It was estimated that the wavelength of the shear wave was far larger than the testing gap involved thus the impact of rubber inertia on shear distribution was negligible [4].

It has long been realized that dynamic heating of a specimen can be significant during testing of a viscoelastic material at large deformation [25]. We monitored the severity of dynamic heating by inserting a fine thermocouple probe (wire diameter 0.125 mm) into the specimen. For the compound BR-C-N299g tested at RT, the maximum temperature rise encountered was about 1.3 °C during a dynamic strain sweep at 1 Hz between $\gamma_0 = 1\%$ and $\gamma_0 = 141\%$ with the strain increment at 4%, about 1 °C during a dynamic time sweep at 1 Hz and $\gamma_0 = 100\%$ for 300 s, and about 11 °C during a dynamic time sweep at 10 Hz and $\gamma_0 = 100\%$ for 60 s. For the compound BR-Silica undergoing similar tests at 0 °C the corresponding temperature rises detected were ~2.2, ~1.4, and ~12.4 °C, respectively. An attempt was also made to display the significance of friction heating during the BPST testing on the wet concrete surface [30]. An identical thermocouple probe was inserted into the rubber slider from a side not in contact with the concrete surface but as close to the sliding edge as possible. No obvious temperature rise was detected for these BR compounds. Water on the concrete surface can probably efficiently cool the thin surface layer of rubber that determines the wet sliding friction.

Because the nonlinear viscoelastic behavior is notably history-dependent, unless otherwise noted the results presented below were obtained from samples exposed to prior large deformation. Whenever possible the comparison made in the same plot for the compounds is based on samples with similar prior test history. All samples experienced at least 5 min resting before being tested again.

Results and discussion

Dynamic moduli

Compound physical properties including viscoelastic behavior are intimately related to the state of filler dispersion in the matrix polymer achieved via intensive mechanical mixing in the internal mixer. Among other factors, the filler dispersion is facilitated by a stronger affinity between filler and polymer, and a weaker attraction between filler particles. It is still difficult to describe quantitatively the characteristically disordered structure of dispersed filler. However, direct visualization of filler dispersion does, to some extent, offer clues

for understanding the compound viscoelastic behavior observed.

The macro-scale filler dispersion is examined with a LOM. Representative images obtained are shown in Fig. 1 for BR-C-N299, BR-C-N299g, and BR-Silica. The worst situation is seen for BR-C-N299g. The size of the conglomerates of undispersed filler particles can reach ~60 μm. Good macro-scale filler dispersion is achieved for all other compounds. For BR-Silica, in the absence of the silane Si69, a strong filler–filler interaction is considered to exist arising from the hydrogen bonding between surface hydroxyl groups from neighboring silica particles. However, this may be interfered by the high temperature (~160 °C) encountered during mixing, the presence of adsorbed moisture on silica surface, which helps to achieve a good macro-scale filler dispersion.

The micro-scale filler dispersion is revealed with an AFM in the tapping mode. The phase images obtained are shown in Fig. 2 for the same three compounds. Clearly finely dispersed filler particles are achieved for all the compounds.

Some typical compound properties are listed in Table 1. According to both DSC tests (thermal T_g) and frequency/temperature Sweep at $\gamma_0 = 0.20\%$ (T at the peak in $G''(T)$ at 1 Hz), the apparent glass transition temperature is higher for compounds BR-C-N339, BR-Silica, and BR-Silica-Si69, because of the use of 10 phr processing oil in them. Additionally, the extra amount of sulfur used to cure BR-Silica leads to the highest glass transition temperature. However, the maximum variation in glass transition temperature is ~5° by either measure.

For the uncured compounds, the amount of bound rubber is only ~7% for BR-C-N299g in comparison to ~30% for BR-C-N299, consistent with expectation and prior data reported in the literature [21]. Graphitization has deactivated the favorable interactions between the normal carbon black and the polymer. According to the tensile test at RT, the unfilled BR-G exhibits a tensile at break of only 1.32 MPa and a strain at break of only ~145%. For all reinforced compounds the tensile at break is higher than 13 MPa and the strain at break is larger than 500%. Therefore a substantial degree of reinforcement is still achieved even with the graphitized filler N299g. On the other hand, the stress–strain behavior is obviously different for BR-C-N299 and BR-C-N299g. For BR-C-N299g, the stress at 300% strain is only 4.2 MPa, the stress at break is 13.4 MPa, and the strain at break is 762%. In contrast, the corresponding values for BR-C-N299 are 10.0 MPa, 20.7 MPa, and 519%, respectively. Such behavior observed is in agreement with the literature [21].

Because of the complexity of the compound systems involved, a definitive account of the thermorheological behavior, even in terms of linear viscoelasticity, is yet to

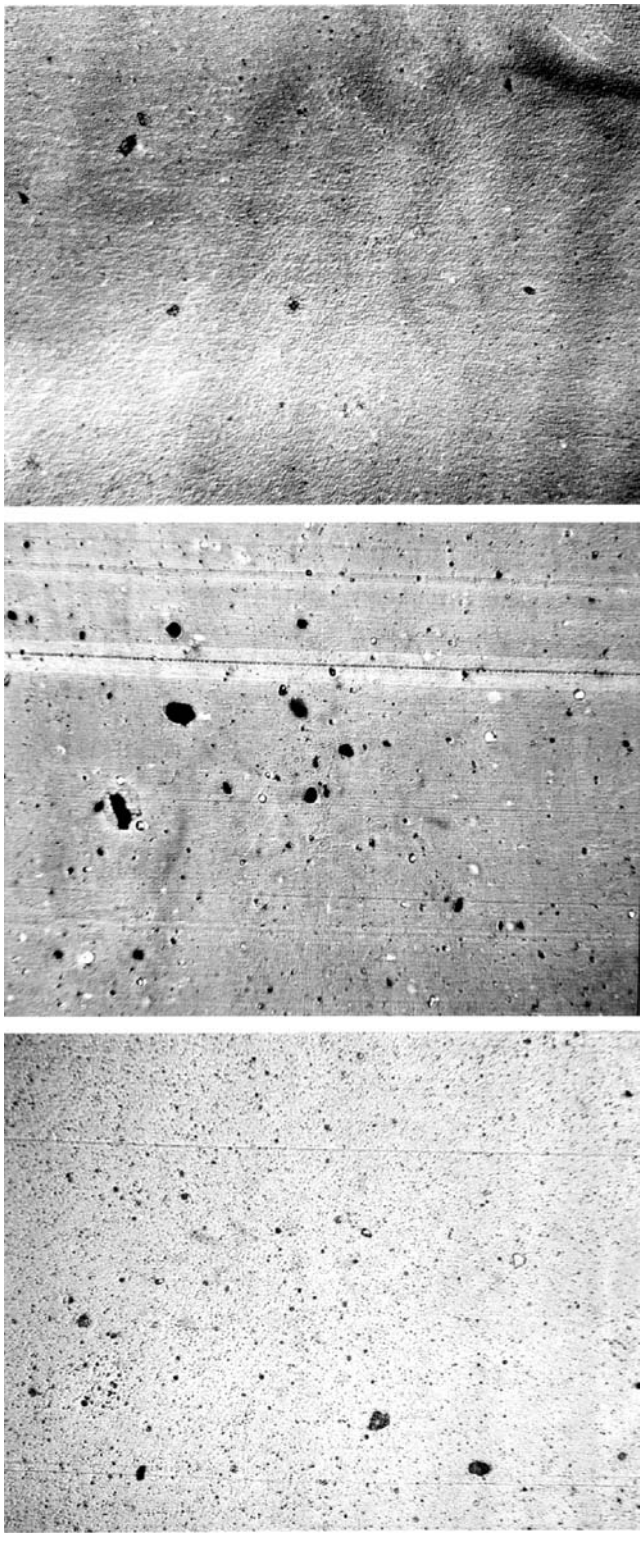

Fig. 1 Light optical microscope images revealing the macro-scale filler dispersion status for BR-C-N299 (*top*), BR-C-N299g (*center*) and BR-Silica (*bottom*). The image width corresponds to 1425 μm

Fig. 2 Atomic force microscope tapping mode phase images revealing the micro-scale filler dispersion status for BR-C-N299 (*top*), BR-C-N299g (*center*) and BR-Silica (*bottom*). The image width corresponds to 4 μm

be established. However, there has appeared the assumption that the difference in the time–temperature shifting behavior between a carbon black-filled compound and a silica-filled compound could be responsible for their difference in wet sliding friction [27]. In this study, time–temperature shifting is uncritically applied for all the compounds. The manual shifting is based on tanδ and horizontal only. Even though the frequency/temperature sweep testing at $\gamma_0 = 0.20\%$ covers a wider temperature range, only data points obtained between −86 and −58°C are employed for shifting. The reference temperature T_r is chosen at −86 °C for all the compounds. This T_r is slightly below the temperature at the peak in $G''(T)$ at 1 Hz for BR-G.

As shown in Fig. 3a for tanδ on a linear scale, the shifting does not lead to a well-superposed master curve. This is most obvious for BR-G: the data points around the peak region are noticeably scattered. In fact, this arises from a decreasing maximum in tan$\delta(f)$ with increasing T, opposite to the trend reported for (uncrosslinked) lower molecular weight polybutadiene of similar microstructure [29]. Such scattering around the peak region is mostly suppressed for the filled compounds. The resulting ''superposed'' curves for G'' are displayed in Fig. 3b on a logarithmic scale for all the compounds. The low frequency portion of $G''(f)$ appears noisier for BR-Silica than for other compounds. It is obvious from Fig. 3 that in terms of tanδ and G'' at small strain, the six compounds can be approximately separated into four groups: (1) BR-G; (2) BR-C-N299 and BR-C-N299g; (3) BR-C-N339 and BR-Silica-Si69; and (4) BR-Silica. The difference in the linear thermorheological behavior comes from the absence of reinforcing filler in BR-G, the usage of 10 phr of oil in BR-C-N339, BR-Silica, and BR-Silica-Si69, and the extra amount of sulfur used to cure BR-Silica.

The corresponding shift factors $a_T(T)$ involved are summarized in Fig. 4 for comparison. The shift factors are affected by the differences among the compounds. Using the shift factors for BR-G as the baseline, then BR-Silica exhibits the most deviation. Such deviation is less for BR-C-N339 and BR-Silica-Si69, and is least for BR-C-N299 and BR-C-N299g. There seems to be only a small difference between the shift factors of BR-C-N339 and BR-Silica-Si69. Among all the filled compounds, BR-C-N299g shows the least amount of bound rubber while its shift factors are closest to those for BR-G. However, even in the presence of a significant amount of bound rubber, the shift factors for BR-C-N299 only

Table 1 Compound properties

Compound	BR-G	BR-C-N339	BR-C-N299	BR-C-N299g	BR-SiO_2	BR-SiO_2-Si69
Bound rubber (%) (uncured)	N/A	23.2	29.7	6.8	22.8	30.6
DSC mid-point T_g (°C)	−86.8	−85.5	−87.4	−87.4	−82.2	−84.7
T@peak G″ at 1 Hz (°C)	−85.7	−83.6	−85.3	−85.2	−80.9	−83.0
Swelling test: V_R	0.19	0.24	0.27	0.23	0.26	0.25
Tensile test at RT:						
Stress at 300% strain (MPa)	N/A	7.04	10.0	4.2	7.27	7.72
Strain at break (%)	145.3	607.9	519.4	762.3	551.2	544.4
Stress at break (MPa)	1.32	18.0	20.7	13.4	14.6	15.7
BPST test at RT: BPN	40.7	47.9	46.5	49.7	50.2	52.0

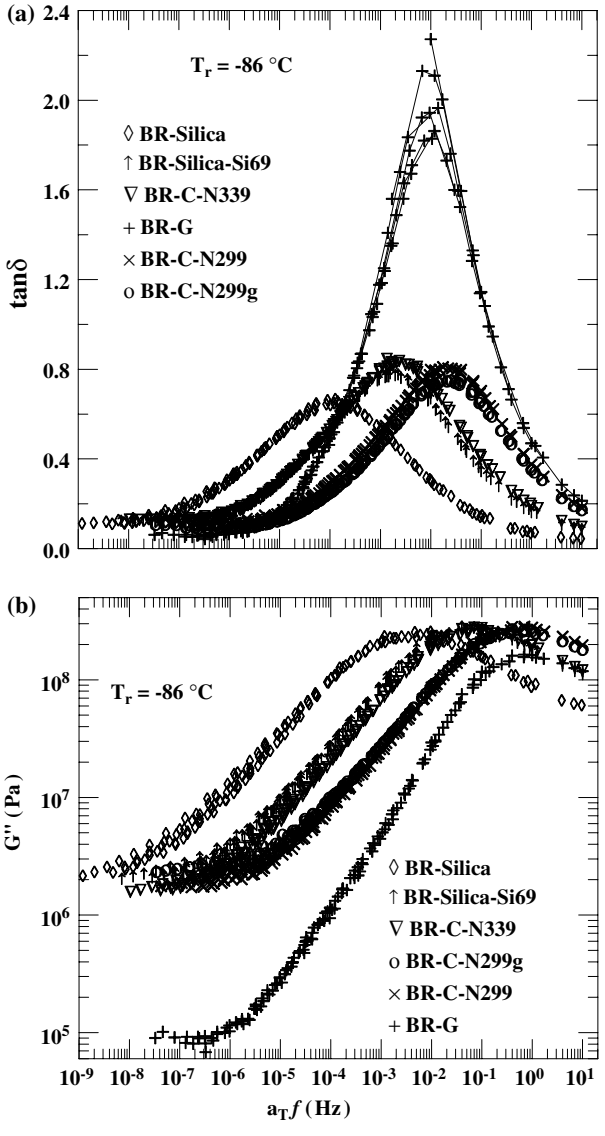

Fig. 3 Mechanical spectrums obtained for the compounds via horizontal-only time–temperature shifting: **a** in terms of tanδ; **b** in terms of G'' as a consequence

deviate slightly more from those for BR-G. As will be shown later, BR-C-N299g already behaves nonlinearly at $\gamma_0 = 0.20\%$. A frequency/temperature sweep test was also performed at $\gamma_0 = 0.05\%$ for BR-C-N299g, and qualitatively similar shifting behavior was obtained, with the shift factors moving closer to those of BR-G.

Considering the large deformation possibly involved during sliding of rubber on a road surface, we are mainly interested in looking at G^* at large strain. Because the reinforced rubber compounds are actually dispersion systems with internal structure (filler networking), the time-dependence of G^* at constant γ_0, or the thixotropic behavior, needs to be examined first for meaningful interpretation of results obtained from tests at large strain. The variations of G' and tanδ with time during a dynamic time sweep at 1 Hz and RT are shown in Fig. 5 for all the compounds. Here, $\gamma_0 = 100\%$ except for BR-G where $\gamma_0 = 50\%$ to avoid possible cracking of the gum compound during testing. The data shown were obtained with fresh samples without prior history of shear deformation. The most obvious time-dependency is observed for BR-Silica, consistent with the perception of a strong filler–filler network in BR-Silica. However,

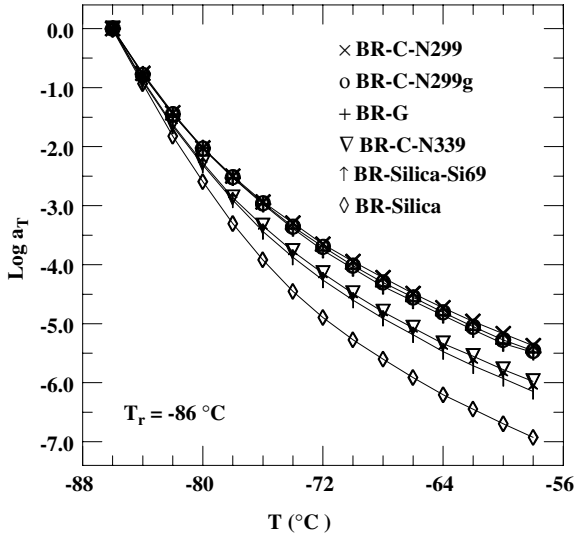

Fig. 4 The shift factors used to obtain Fig. 3

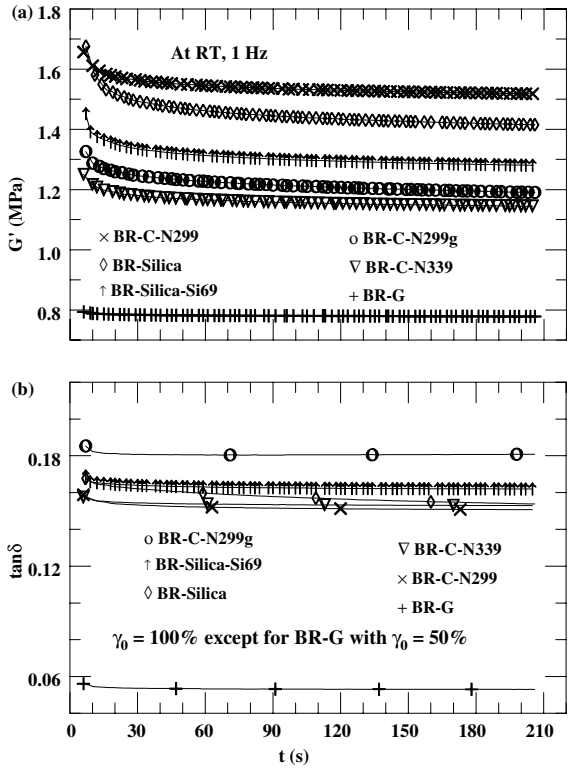

Fig. 5 Variation of G^* with time during a dynamic time sweep at 1 Hz and RT. For clarity, not every data point labeled

other than at the beginning of testing, the overall time-dependency is not significant; and such time-dependency becomes less for samples with prior history of large shear deformation. The rankings in G' or tanδ at times beyond the initial time-dependent zone are consistent with those from a dynamic strain sweep at 1 Hz, RT and at similar γ_0 (not shown).

The variation of G' with γ_0 at 1 Hz and 0°C is shown in Fig. 6 for $\gamma_0 \leq 30\%$. For all the dynamic strain sweep tests, at each γ_0 two cycles of oscillation were applied first and the measurement was taken during the third cycle of oscillation. It is rather striking to observe that G' at small γ_0 is substantially higher for BR-C-N299g than for all other compounds despite the fact that BR-C-N299g has the worst macro-scale filler dispersion. One would expect a somewhat higher value for BR-Silica because of the highest T_g and strong filler–filler interactions, because of hydrogen bonding between neighboring particles in the absence of the silane Si69. It was discovered later in a very recent report [18] that a similar contrast was detected in G' at small γ_0 between a carbon black-filled compound and a compound filled with the corresponding graphitized carbon black. Reduction in G' with increasing γ_0 is already obvious at $\gamma_0 = 0.1\%$ for BR-C-N299g. In contrast, for other filled compounds, such reduction becomes obvious only at $\gamma_0 \geq 0.2\%$. On the same linear scale, the reduction in G' with γ_0 is hardly perceptible for BR-G.

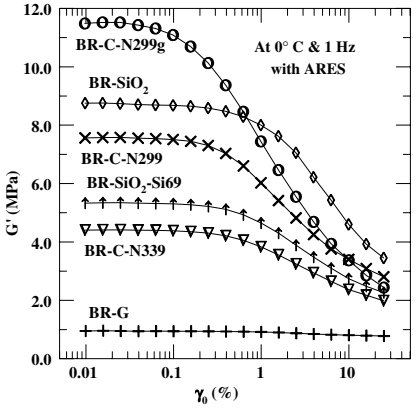

Fig. 6 Nonlinear variation of G' with strain for $\gamma_0 \leq 30\%$ tested at 1 Hz and 0°C

The results obtained from linear dynamic strain sweep tests at 1 Hz, 0°C and between $\gamma_0 = 1\%$ and $\gamma_0 = 141\%$ with a step increment of 4% are displayed in Fig. 7. Overall G' keeps decreasing with increasing γ_0. This decrease is most rapid for $\gamma_0 \lesssim 10\%$ while for $\gamma_0 \gtrsim 30\%$ the rate of decrease becomes obviously smaller. For $\gamma_0 > 60\%$, the order from high to low in G' is BR-C-N299 > BR-Silica > BR-Silica-Si69 > BR-C-N339, and the decreasing $G'(\gamma_0)$ remains more or less parallel to each other among them. In contrast, G' for BR-C-N299g is larger than all other compounds for $\gamma_0 \leq 0.5\%$ while at the maximum γ_0 tested ($\sim$140%) G' for BR-C-N299g becomes almost the same as the value for BR-C-N339 but appears to be decreasing at a faster rate. Even considering there is 10 phr of oil in BR-C-N339 and BR-Silica-Si69, this unique behavior of BR-C-N299g at large γ_0 probably arises from the shortage of bound rubber on graphitized carbon black. Testing at 1 Hz and RT demonstrates similar characteristics for the compounds.

In Fig. 7b we observe that tanδ for BR-C-N339, BR-C-N299, and BR-Silica-Si69 increases at small γ_0, reaches a maximum at $\gamma_0 \sim 5\%$, then decreases for $5\% \lesssim \gamma_0 \lesssim 40\%$, and becomes more or less constant for $\gamma_0 \gtrsim 40\%$. Compounds BR-C-N299g and BR-Silica behave differently. For BR-C-N299g, tanδ still reaches a maximum at $\gamma_0 \sim 5\%$; however, it starts to increase again for $\gamma_0 \gtrsim 30\%$. For BR-Silica, the maximum in tanδ appears at $\gamma_0 \sim 16\%$, and the peak appears rather blunt. Afterwards, tanδ keeps decreasing with γ_0. It must be emphasized that the results shown here were obtained with samples exposed to prior large shear deformation. The first run of a dynamic strain sweep on a fresh sample gives quantitatively different but qualitatively similar results. Upon repeated testing, the quantitative difference between two consecutive runs gradually decreased. The difference between the first run and the second run was most obvious for BR-Silica.

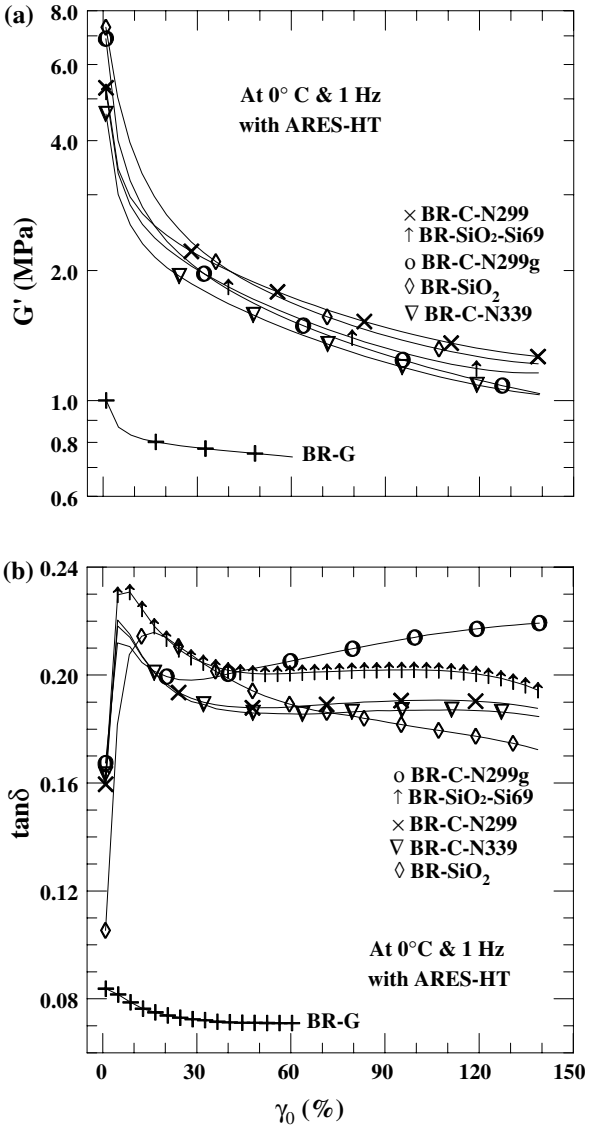

Fig. 7 Nonlinear variation of G^* with strain for $\gamma_0 \leq 141\%$ tested at 1 Hz and 0 °C: **a** in terms of G'; **b** in terms of tanδ. For clarity, not every data point labeled

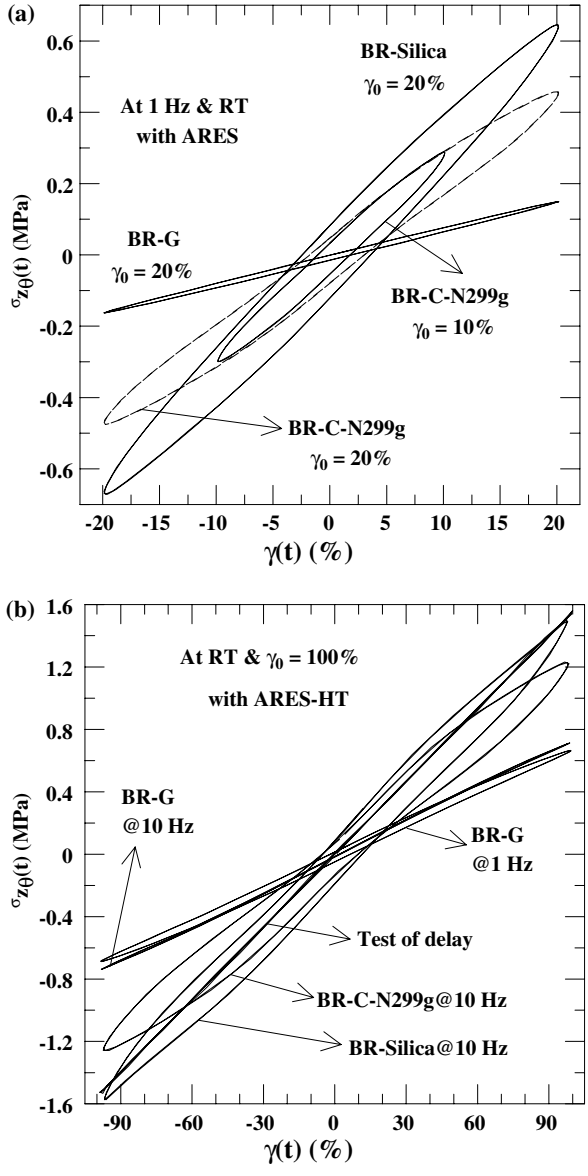

Fig. 8 Trajectories of shear stress vs. shear strain corresponding to the fifth and sixth cycles of strain variation at RT: **a** for $\gamma_0 \leq 20\%$; **b** for γ_0 at 100%

At 1 Hz, 0°C and $\gamma_0 = 0.01\%$, G' is 0.95 MPa for BR-G whereas G' lies between 4.4 and 11.5 MPa for the filled compounds. In contrast, G' is 0.74 MPa for BR-G at $\gamma_0 = 60\%$ and lies between 1.03 and 1.26 MPa for the filled compounds at $\gamma_0 \sim 140\%$. Therefore, the difference in G' between a gum compound and a reinforced compound or among the compounds filled with different reinforcing fillers becomes much diminished at large γ_0.

Analysis of higher harmonic excitation was performed on signals acquired during arbitrary waveform tests. Typically ten cycles of oscillatory shear strain at the desired γ_0 and f were imposed. If the stress $\sigma(t)$ is plotted against the strain $\gamma(t)$, the response from a linear viscoelastic material adheres to an elliptical trajectory. A non-elliptical trajectory indicates deviation from linear viscoelasticity. Typical trajectories corresponding to the fifth and sixth cycles of $\gamma(t)$ obtained for the compounds at different γ_0 are shown in Fig. 8. From Fig. 8a, the deviation from an elliptical trajectory is apparent for BR-C-N299g even at $\gamma_0 = 10\%$. In contrast, the deviation is not obvious for BR-G and BR-Silica at $\gamma_0 = 20\%$. Fig. 8b shows that the trajectories for filled compounds become clearly non-elliptical at large γ_0.

Different signals are actually acquired in a sequential manner by the data-acquisition system. It is important

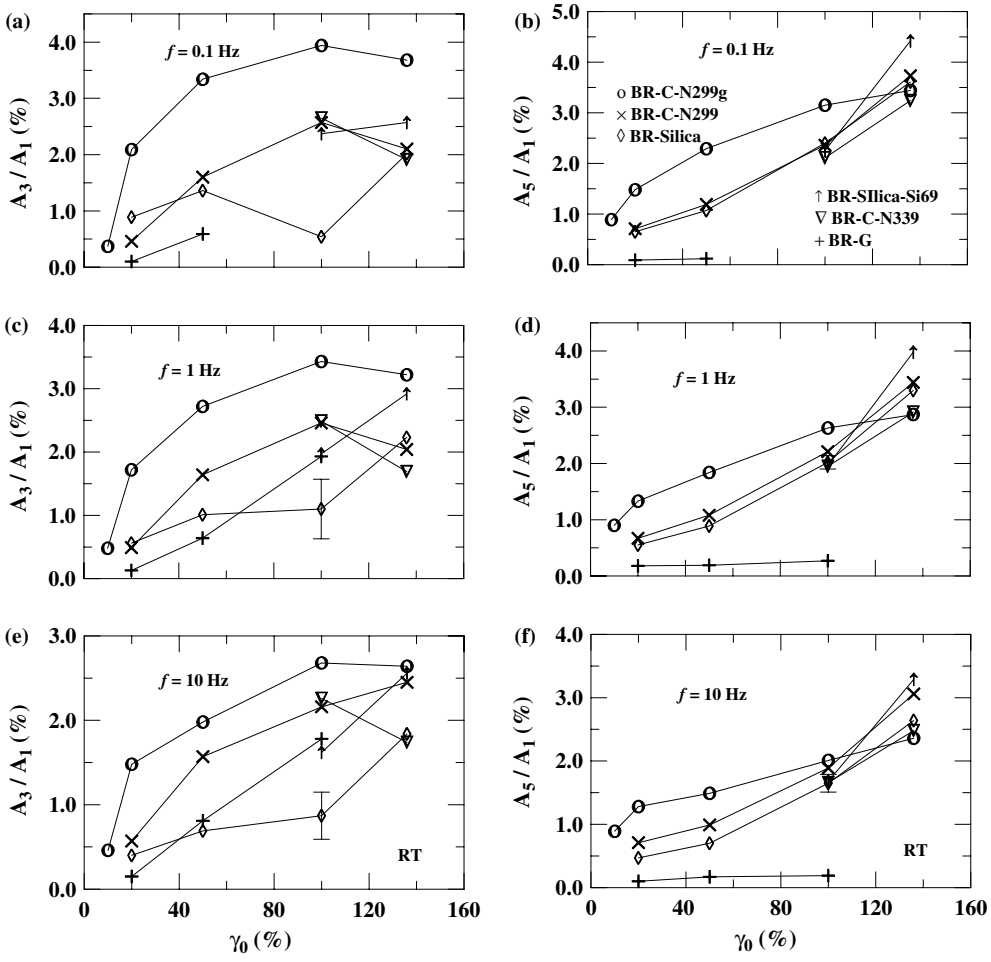

Fig. 9 Variation of the stress amplitude at the third or fifth harmonic (normalized with respect to that for the fundamental) with γ_0 at RT. The error bar indicating the standard deviation in **c** and **d** is based on testing three different samples while the error bar in **e** and **f** is from testing two different samples

to correct for the time delay between neighboring channels [28]. To reveal any possible residual effect from such correction via data interpolation, the sinusoidal strain at 10 Hz and $\gamma_0 = 100\%$ is recorded by both the "stress channel" and the "strain channel" of the data-acquisition system. The corrected trajectory is displayed in Fig. 8b and labeled with "test of delay". Clearly the deviation from the ideal straight line expected is minimal.

The data-acquisition system decides the exact data-sampling rate. The total data-sampling rate for three acquisition channels (torque, strain, normal force) is about 122 Hz for $\gamma(t)$at $f = 0.1$ and 1 Hz, and about 976 Hz for $\gamma(t)$ at $f = 10$ Hz. To analyze the harmonic content in strain and stress waveforms via FFT the raw data points (after correction for the time-delay) are interpolated so that the number of data points corresponding to one cycle of strain is an integral power of 2. The commercial software Origin was employed for all these operations. Analysis of the strain waveforms at different f and γ_0 reveals that the amplitude of the higher harmonics is typically less than 0.1% of the amplitude at the fundamental frequency. Only in a few cases (mostly at $f = 10$ Hz) does the amplitude for certain higher harmonics exceed 0.1%, although it still remains below 0.5% of the amplitude at the fundamental frequency. Therefore the higher harmonic content is insignificant in the strain waveform.

The analysis of the higher harmonic excitation in the stress waveform in response to the imposed sinusoidal strain is summarized in Fig. 9. Up to the maximum strain of 136% studied, the extent of higher harmonic excitation is still small. However, the presence of higher harmonics is definite, and some unexpected features are observed. In discussion below regarding the higher harmonic content in the stress response, A_1 is used to denote the amplitude at the fundamental frequency while A_n denotes the amplitude at n times the fundamental frequency with $n \geq 2$. Even though the results indicate the unexpected presence of a non-trivial second harmonic ($0.10\% \leq A_2/A_1 \leq 0.60\%$) in many cases, it is the third and fifth harmonics that become dominant at large γ_0. For BR-C-N299g, even the seventh and the ninth harmonics can become non-trivial (with A_7/A_1 as

large as 1.1%) at large γ_0 and especially at $f = 0.1$ Hz. Variations of A_3/A_1 and A_5/A_1 with γ_0 are shown in Fig. 9 at different excitation frequencies.

The most distinct difference between a gum compound and a filled compound is in the relative strength of the third and the fifth harmonics. For filled compounds, $A_3 \sim A_5$ or even $A_3 < A_5$ in many cases, whereas A_5/A_1 remains very small for the gum compound. For BR-G, A_3/A_1 clearly increases with increasing γ_0 and becomes similar in magnitude to that of the filled compounds at large γ_0. The compound BR-C-N299g has the largest A_3/A_1 among all the compounds up to the maximum γ_0 at 136% tested. However, its initial trend of increasing A_3/A_1 with γ_0 levels off at large γ_0. For all the filled compounds, A_5/A_1 increases with increasing γ_0; however, the rate of increase for BR-C-N299g becomes less than that for other filled compounds at large γ_0.

Results obtained for all the compounds at $\gamma_0 = 100\%$ are compiled together in Fig. 10 to demonstrate the variation of A_3/A_1 and A_5/A_1 with f. We can see an overall trend of decreasing A_3/A_1 and A_5/A_1 with increasing f, most prominent for BR-C-N299g.

In the presence of static shear γ_m superposed in parallel to the oscillatory shear strain, the even harmonic components emerge in the stress response. Tests were run at RT with the excitation frequency at 1 Hz. Variation of A_n/A_1 with γ_0 is shown in Fig. 11 for BR-Silica with $\gamma_m = 20\%$. The plot also displays the higher harmonic content at $\gamma_0 = 50\%$ with γ_m at either 50% or 80%. Results for BR-C-N299 and BR-C-N299g with $\gamma_m = 20\%$ and $\gamma_0 = 100\%$ are also compared. These results are obtained from the stress response during the second cycle of oscillatory strain. In changing from the second cycle to the ninth cycle of strain, a small change in A_n/A_1 is detected while the structure of the higher harmonics remains the same. We can see from Fig. 11 that under all the conditions investigated A_n/A_1 is no more than 6%. In most cases, the second harmonic is the strongest of the higher harmonics.

We mention here in passing that the magnitude of higher harmonics excited seems more significant under oscillatory compressional deformation than under oscillatory shear deformation. Rubber cylinders of diameter 9.4 mm and height 15.5 mm were tested with an MTS instrument. A sinusoidal displacement of amplitude 2.0 mm at $f = 1.0$ Hz was superposed in parallel onto a static compressional displacement of 5.0 mm. Analysis of the displacement signal reveals insignificant higher harmonic content. However, for a butyl gum compound, analysis of the load signal reveals that $A_2/A_1 = 10.9\%$, $A_3/A_1 = 1.6\%$, and $A_4/A_1 = 0.36\%$. For a butyl compound filled with 50 phr of N339 and containing no oil, the corresponding values become 16.5,

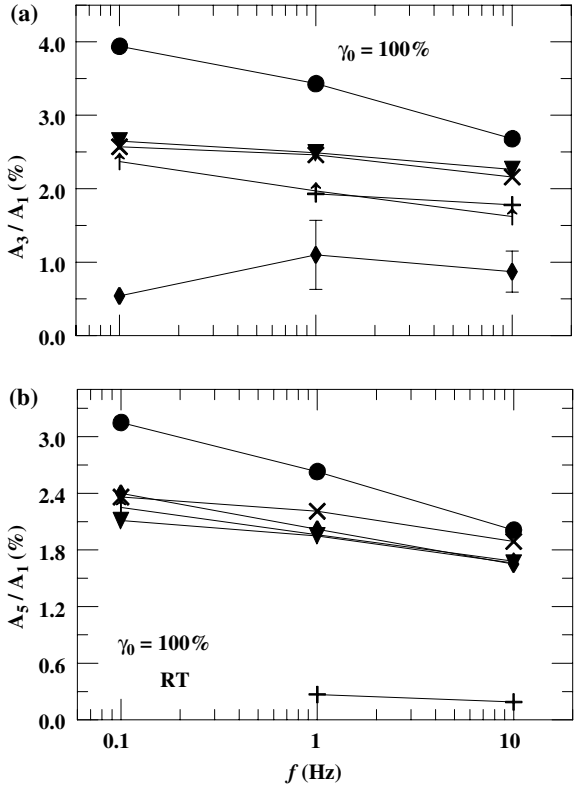

Fig. 10 Variation of the stress amplitude at the third or fifth harmonic (normalized with respect to that for the fundamental) with f at $\gamma_0 = 100\%$ and RT

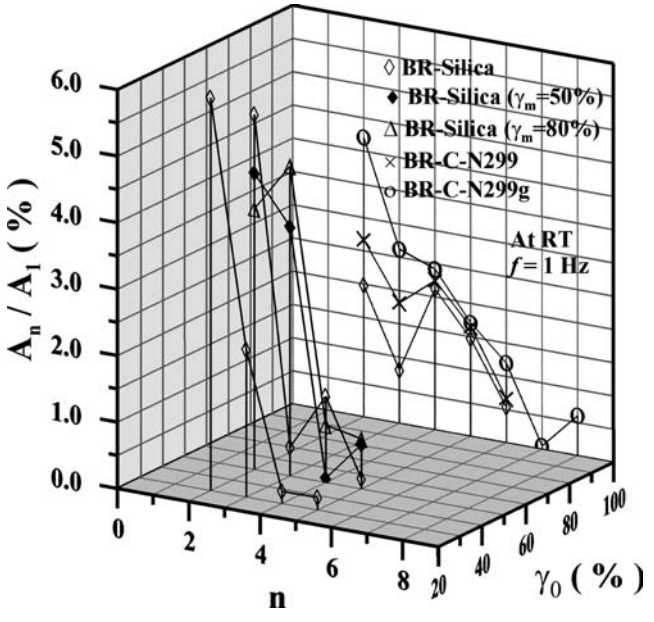

Fig. 11 Higher harmonic content in the presence of a static shear strain γ_m superposed in parallel. The strain excitation is at 1 Hz and RT. Other than the two cases specified in the plot, $\gamma_m = 20\%$

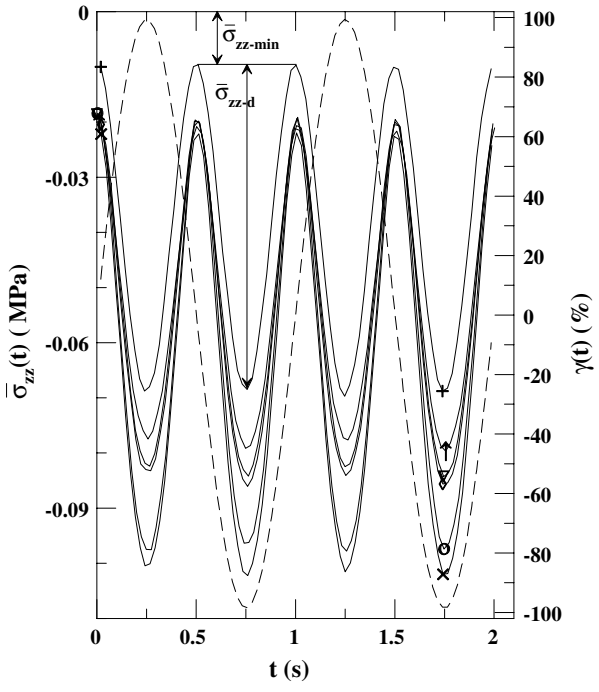

Fig. 12 The average normal stress waveform during the fifth and sixth cycles of strain $\gamma(t)$ at $\gamma_0 = 100\%$, 1 Hz and RT. The *dashed line* indicates $\gamma(t)$. The signs labeling the waveforms are used in the same way as in other figures

6.8, and 2.2%, respectively. For BR-G, the corresponding values are 9.0, 0.89, and 0.15%, respectively.

The normal force response has rarely been characterized for elastomer compounds. However, for a thorough description of the viscoelastic behavior, this should not be ignored. During the arbitrary waveform tests performed, the normal force generated pushes against the upper plate and the corresponding signal recorded remains negative. It is known that for the Lodge rubber-like liquid under oscillatory strain, the first normal stress difference is given by:

$$N_1(t) = \sigma_{rr} - \sigma_{zz} = \gamma_0^2[G'(\omega) - B(\omega)\cos(2\omega t) - C(\omega)\sin(2\omega t)],$$

here $B(\omega)$ and $C(\omega)$ are integral transforms of the memory function [9]. It is therefore expected that $N_1(t)$ oscillates at twice the frequency of the strain excitation and that there is a nonzero offset equal to $\gamma_0^2\, G'(\omega)$.

Here we define an average normal stress $\bar{\sigma}_{zz}$ as the total normal force detected along the axis of rotation, F, divided by the cross-sectional area of the parallel plate geometry. The $\bar{\sigma}_{zz}$ waveform during the fifth and sixth cycles of strain at 1 Hz, $\gamma_0 = 100\%$, and RT is displayed in Fig. 12 for all the compounds. Clearly $\bar{\sigma}_{zz}$ oscillates twice as fast as $\gamma(t)$. Two quantities are also defined in Fig. 12: $\bar{\sigma}_{zz-min}$ as the minimum in $\bar{\sigma}_{zz}$ during oscillation, and $\bar{\sigma}_{zz-d}$ as the peak-to-peak amplitude of oscillation for $\bar{\sigma}_{zz}$. The gum compound BR-G has the weakest $\bar{\sigma}_{zz-min}$. Compounds BR-C-N339, BR-Silica, and BR-Silica-Si69 have a similar $\bar{\sigma}_{zz-d}$, in comparison to a stronger $\bar{\sigma}_{zz-d}$ for the compounds BR-C-N299 and BR-C-N299g. This is most probably because of the absence of 10 phr oil in the last two compounds.

Qualitative variations of $\bar{\sigma}_{zz-min}$ and $\bar{\sigma}_{zz-d}$ with γ_0 and f are presented in Fig. 13. It is observed that both $\bar{\sigma}_{zz-min}$ and $\bar{\sigma}_{zz-d}$ increase with γ_0. Second-order polynomial fitting has been applied to the dependence on γ_0 in Fig. 13a and b, except for BR-G. In Fig. 13c, $\bar{\sigma}_{zz-min}$ mostly increases with f; in contrast, a slight decrease in $\bar{\sigma}_{zz-d}$ with increasing f can be seen in Fig. 13d for all the compounds presented.

Wet sliding friction

An typical surface roughness profile as obtained with the Surfanalyzer on the concrete surface is shown in Fig. 14a. It has been converted into the time trace of the vertical displacement that would be experienced by one point at the edge of a slider moving at 2 m s^{-1}. The amplitude spectrum after a Fourier transform, applied to the whole or a portion of the roughness profile, is displayed in Fig. 14b. Obviously the dynamic deformation of rubber during sliding consists of components at many frequencies.

By design, the nominal contact pressure between the slider and the road surface during BPST testing is about 0.2 MPa [11]. However, employing the technique of photographic emulsions, pressures between tire and road with sharp projections up to 55 MPa have been detected [10]. The dynamic contact pressure between a rubber slider and the concrete surface during the BPST testing has been revealed in a similar manner by using Pressurex pressure-indicating films suitable for different pressure ranges. The most obvious impression is obtained with the "UltraLow" film for pressure between 0.19 and 0.59 MPa, the impression becomes less and finer with the "Medium" film for pressure between 9.65 and 48.95 MPa, and more so with the "High" film for pressure between 48.95 and 127.6 MPa. As an example, two scanned images of the same piece of "Medium" film before and after being slid over by BR-C-N339 are displayed in Fig. 15. Here for clear visualization of the impression, a negative image is produced using a photo editor, and adjustments are made to the brightness and contrast. It seems that the impression is affected by compound hardness; however, even the gum compound BR-G still causes impression on the "High" film. Certainly the exact contact mechanics between the rubber slider and the concrete surface has been altered due to the presence of the Pressurex film in-between. Furthermore, as the slider moves over the glossy side of the Pressurex film, the sliding dynamics have also been

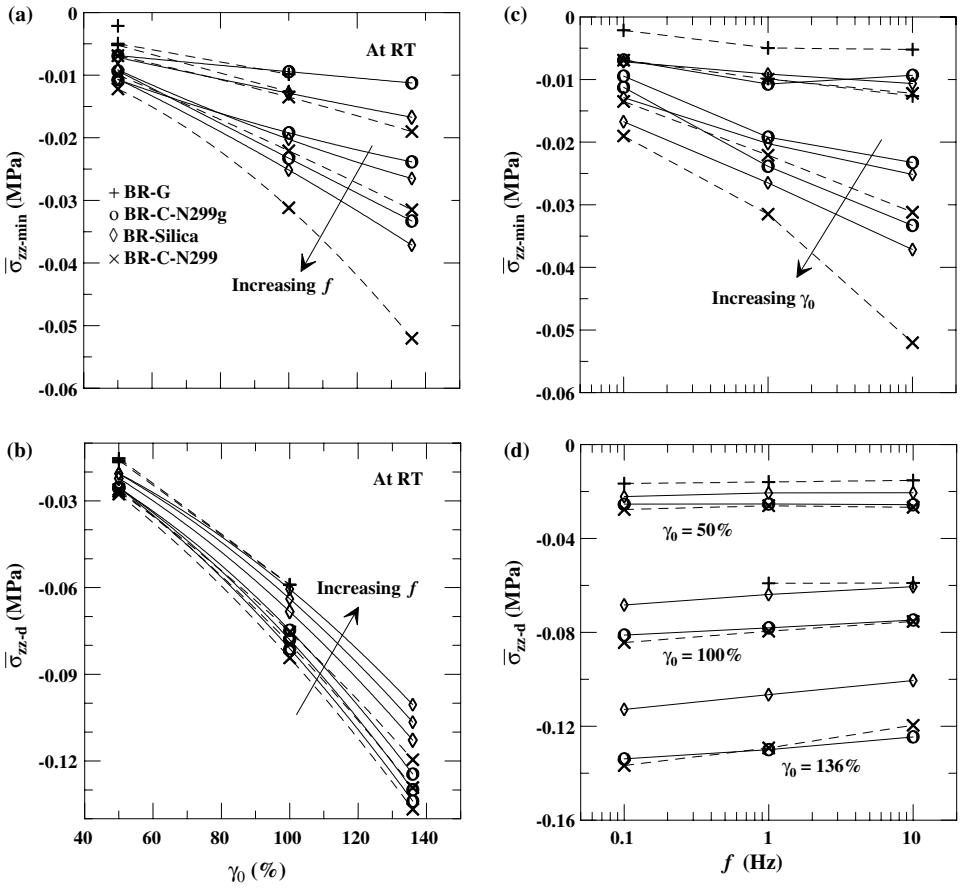

Fig. 13 Variation of the average normal stress with γ_0 or f

modified by what is conventionally termed adhesion contribution, strong on a smooth surface. The stick-slip movement can be clearly seen in Fig. 15b.

The BPN obtained at RT for each compound is shown in Table 1. This BPN is normalized with respect to the value for BR-C-N339 and displayed in Fig. 16. In the rubbery state, the existence of a filler network causes enhanced energy dissipation and contributes positively to the wet sliding friction. As clearly shown in Fig. 16, different filler does cause difference in wet sliding friction. Here silica leads to the highest BPN while the graphitized carbon black is better than the usual carbon black for wet sliding friction.

For BR-C-N339, BR-Silica, and BR-Silica-Si69, the variation of BPN with T is examined between ~0 and ~39 °C in Fig. 17. Overall, BPN decreases with increasing T. The difference between BPN for silica-filled compounds and BPN for carbon black-filled compounds persists in the temperature range tested. There seems to be an indication that BPN for BR-Silica-Si69 is slightly higher than that for BR-Silica; however, this difference is not always reproduced.

For rubber sliding on a wet road surface, systematic presentation of the friction trend as a Stribeck curve [17, 39], which displays the variation of the friction force or friction coefficient with the Summerfeld number (sliding speed×bulk liquid viscosity/load), has yet to appear. How the Stribeck curve is affected by the change in reinforcing filler or compound viscoelasticity is unknown. When temperature increases from 0 to 40°C, the viscosity of water reduces by a factor of 2.7 [24]. So does the Sommerfeld number for the BPST testing. However, for BR-G [30], BR-C-N339, BR-Silica, and BR-Silica-Si69, BPN decreases with increasing T between 0 and 40°C. This suggests that the wet sliding during the BPST testing employed here is in the boundary lubrication regime, and the friction is determined by the material properties of the rubber compounds.

Unfortunately the detailed viscoelastic characterization described above is still insufficient to explain the different wet sliding friction arising from different reinforcing fillers. According to Fig. 4 the linear thermorheological behavior seems to be more affected by the presence of oil and the crosslink density than by the type of filler. At large strain, the difference in G' among the reinforced compounds becomes much diminished (Fig. 7a). The ranking in BPN among the compounds as displayed in Figs. 16 and 17 is inconsistent with the

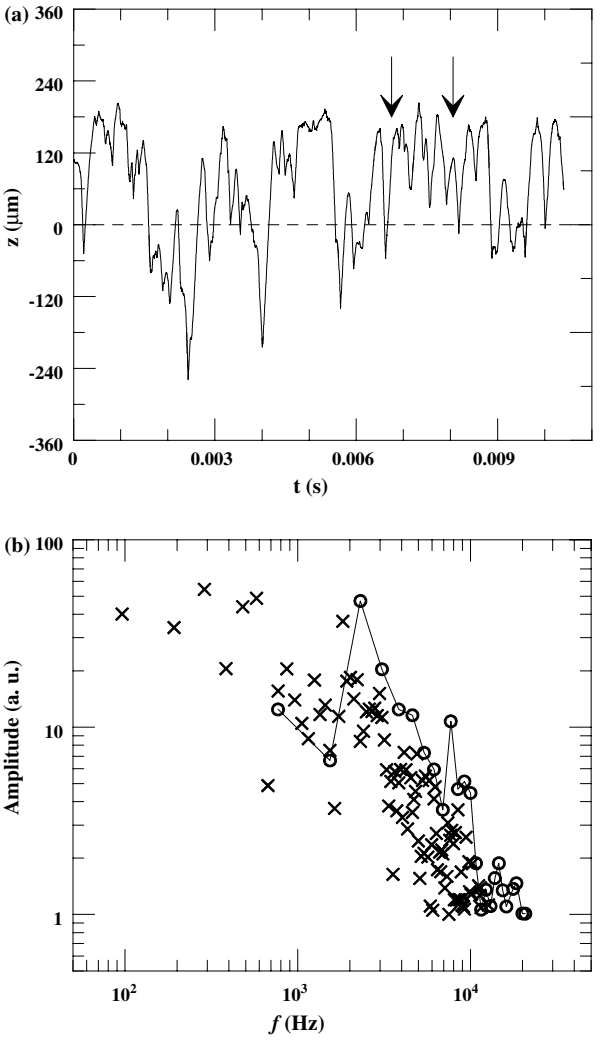

Fig. 14 Typical surface roughness profile obtained with the Surfanalyzer: **a** converted to the vertical displacement as would be experienced by one point at the edge of a slider moving at 2 m s^{-1}; **b** the corresponding amplitude spectrum after applying the Fourier transform. The *empty circular signs* in **b** indicate the spectrum for the portion of the roughness profile between the *two arrows* in **a**

ranking in tanδ at large γ_0 (~100%) obtained from the dynamic strain sweep test at 0°C (Fig. 7b) or the dynamic time sweep test at RT (Fig. 5b). The difference between higher harmonic excitation under shear deformation for the carbon black-filled compounds and that for the silica-filled compounds is unremarkable (Fig. 9). On the other hand, the ranking in tanδ at γ_0 between 20 and 30% as shown in Fig. 7b seems to be in agreement with the ranking in BPN among the compounds. However, the dynamic strain sweep tests at 1 Hz and RT reveals a different ranking in tanδ between $\gamma_0 = 20$ and $\gamma_0 = 30\%$ among the compounds while the difference in BPN persists between ~0 and ~39 °C on the Portland cement concrete surface.

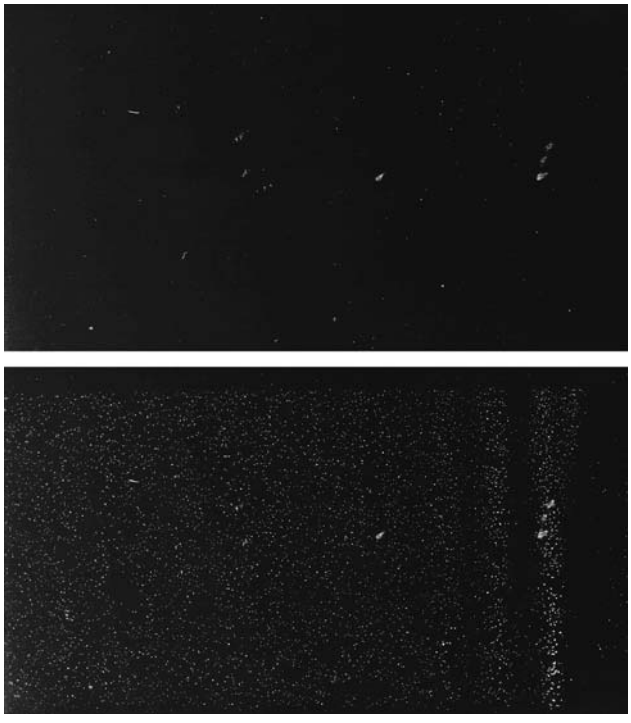

Fig. 15 Impression of contact pressure (between 9.65 and 48.95 MPa) generated by the rubber slider for BR-C-N339 during single BPST testing: **a** scanned image before testing; **b** scanned image after testing. The slider slides from right to left on the glossy slide of a piece of Medium Pressurex pressure indicating film covering the dry concrete surface. The image height in **b** corresponds to 80 mm

Conclusion

In pursuit of a better understanding of the relationship between wet sliding friction of rubber compounds and

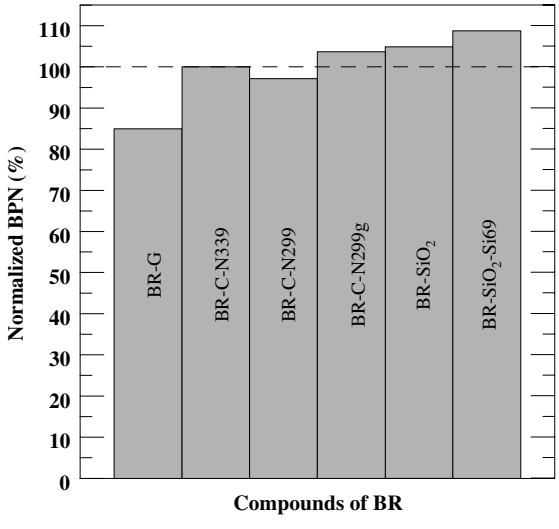

Fig. 16 BPN for all the compounds at RT normalized relative to the value for BR-C-N339

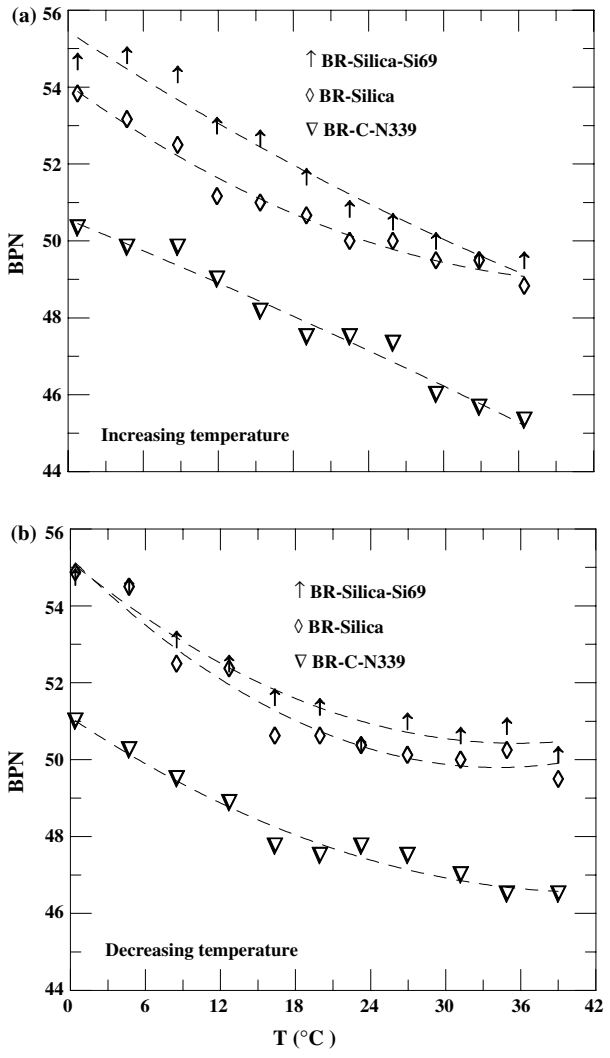

Fig. 17 Variation of BPN with temperature for BR-C-N339, BR-Silica, and BR-Silica-Si69

their bulk viscoelastic properties, especially the contribution from different reinforcing fillers, we examined in detail the linear thermorheological behavior, the nonlinear dynamic moduli under shear deformation, and the wet sliding friction of crosslinked rubber compounds made of a low-*cis* polybutadiene and reinforced with different reinforcing fillers (carbon black, graphitized carbon black, and precipitated silica). The scenario of possible extra energy dissipation via higher harmonic excitation in rubber compounds coupled with dynamic deformation consisting of components at many frequencies during sliding of rubber on a rough surface was considered. Overall, up to the maximum strain amplitude of ~140% tested, there seems no straightforward explanation relating the observed difference in wet sliding friction as a result of the different fillers to the bulk viscoelastic properties of the rubber compounds.

On the other hand, many interesting features were observed from the viscoelastic characterization covering a wide range of strain. The filled compounds are differentiated from the unfilled compound in the simultaneous excitation of the third and fifth harmonics of similar magnitude in stress in response to an imposed sinusoidal shear strain. Among all the filled compounds, the compound filled with graphitized carbon black had the largest storage modulus at small strain, a resurgence of loss tangent at large strain, and the fastest rate of decrease in storage modulus with strain persisting to the maximum strain tested. Such characterization is undoubtedly helpful for further advancing our understanding of filler reinforcement behavior.

Finally it worth pointing out that the magnitude of the higher harmonics excited seems more significant under oscillatory compressional deformation than that under oscillatory shear deformation. For better understanding on the relationship between bulk viscoelastic properties and wet sliding friction of rubber compounds, the effects of reinforcing filler on higher harmonic excitation under oscillatory compressional deformation need to be systematically investigated.

Acknowledgements The permission of Bridgestone/Firestone North American Tire, LLC, to publish this work is much appreciated. I received generous help from numerous people during the course of this study. I am particularly indebted to the following individuals: Dr L. Nikiel at Sid Richardson Carbon Co. for providing samples of N299 and N299g and the relevant data; Mr J.T. Wilson and Dr M.T. Arigo for using the Surfanalyzer system; Mr B.M. Cernik for taking the LOM images; Mr E.D. Kelley for help with the rheometers; Dr M.W. Hayes for DSC, GPC, and bound rubber tests; Mr D.R. Brumbaugh for the NMR test; and Dr M.T. Arigo for patient help on manuscript revision.

Appendix A: Compounding formula

Table 2 lists the compounding formula. Here the antidegradant 6PPD is *N*-(1,3-dimethylbutyl)-*N*′-phenyl-*p*-phenylenediamine. The bifunctional, sulfur-containing organosilane Si69, or bis(triethoxysilylpropyl)tetrasulfane, is carried on particles of carbon black N330 at the weight ratio 50:50 (a commercial product X 50-S from Degussa). The vulcanization accelerators DPG, MBTS, and TBBS represent diphenyl guanidine, dibenzothiazyl disulfide, and *N*-*tert*-butyl-2-benzothiazyl sulfenamide, respectively.

Table 2 Compounding formula

Compound	BR-G	BR-C-N339	BR-C-N299	BR-C-N299g	BR-SiO_2	BR-SiO_2-Si69
Master batch (phr)						
Low-*cis* BR	100	100	100	100	100	100
N339	0	50	0	0	0	0
N299	0	0	50	0	0	0
N299g	0	0	0	50	0	0
Silica	0	0	0	0	50	50
Oil Sundex790	0	10	0	0	10	10
Stearic acid	2.0	2.0	2.0	2.0	2.0	2.0
6PPD	1.0	1.0	1.0	1.0	1.0	1.0
Remill (phr)	N/A	Yes	Yes	Yes	Yes	Yes
X 50-S	0	0	0	0	0	10
Final batch (phr)						
Zinc oxide	3.0	3.0	3.0	3.0	3.0	3.0
DPG	0.5	0.5	0.5	0.5	0.5	0.5
MBTS	1.0	1.0	1.0	1.0	1.0	1.0
TBBS	0	0	0	0	1.0	1.0
Sulfur	1.3	1.3	1.3	1.3	3.0	1.15

References

1. ASTM E303-93 (1993) Standard test method for measuring surface frictional properties using the British pendulum tester
2. Bevilacqua EM, Percarpio EP (1968) Friction of rubber on wet surfaces. Science 160:959–964
3. Chazeau L, Brown JD, Yanyo LC, Sternstein SS (2000) Modulus recovery kinetics and other insights into the Payne effect for filled elastomers. Polym Compos 21:202–222
4. Darby R (1976) Viscoelastic fluids. Marcel Dekker, New York
5. Davis WM, Macosko CW (1978) Nonlinear dynamic mechanical moduli for polycarbonate and PMMA. J Rheol 22:53–71
6. French T, Patton RG (1963) Advances in roadholding characteristics of car tyres. In: Messenger TH (ed) Proceedings of the fourth rubber technology conference. Institution of the Rubber Industry, London, pp 196–216
7. Fujimaki T, Morita K (1999) Recent patents on silica reinforced polymers. Int Polym Sci Technol 26:26–34
8. Ganeriwala SN, Rotz CA (1987) Fourier transform mechanical analysis for determining the nonlinear viscoelastic properties of polymers. Polym Eng Sci 27:165–178
9. Giacomin AJ, Dealy JM (1993) Large-amplitude oscillatory shear. In: Collyer AA (ed) Techniques in rheological measurement. Chapman and Hall, London, pp 99–121
10. Giles CG, Sabey BE (1951) The effect of pressure and friction on photographic emulsions. Br J Appl Phys 2:174
11. Giles CG, Sabey BE, Cardew KHF (1962) Development and performance of the portable skid-resistance tester. In: Symposium on skid resistance, special technical publication no. 326. American Society for Testing and Materials, Philadelphia, pp 50–74
12. Greenwood JA, Minshall H, Tabor D (1961) Hysteresis losses in rolling and sliding friction. Proc R Soc Lond A 259:480–507
13. Grosch KA (1963) The relation between the friction and viscoelastic properties of rubber. Proc R Soc Lond A 274:21–39
14. Grosch KA (1996) The rolling resistance, wear and traction properties of tread compounds. Rubber Chem Technol 69:495–568
15. Heinrich G, Dumler HB (1998) Wet skid properties of filled rubbers and the rubber-glass transition. Rubber Chem Technol 71:53–61
16. Heinrich G, Klüppel M (2002) Recent advances in the theory of filled networking in elastomers. Adv Polym Sci 160:1–44
17. Israelachvili JN, Berman AD (1999) Surface forces and microrheology of molecularly thin liquid films. In: Bhushan B (ed) Handbook of micro/nano tribology, Chap. 9, 2nd edn. CRC Press, Boca Raton, pp 371–432
18. Klüppel M (2003) The role of disorder in filler reinforcement of elastomers on various length scales. Adv Polym Sci 164:1–86
19. Klüppel M, Heinrich G (2000) Rubber friction on self-affine road tracks. Rubber Chem Technol 73:578–606
20. Kraus G (1971) Reinforcement of elastomers by carbon black. Adv Polym Sci 8:155–237
21. Kraus G (1977) Reinforcement of elastomers by carbon black. Angew Makromol Chem 60/61:215–248
22. Leblanc JL, de la Chapelle C (2003a) Updating a torsional dynamic rheometer for Fourier transform rheometry on rubber materials. Rubber Chem Technol 76:287–298
23. Leblanc JL, de la Chapelle C (2003b) Characterizing gum elastomers by Fourier transform rheometry. Rubber Chem Technol 76:979–1000
24. Lide DR (1998) CRC handbook of chemistry and physics, 79th edn. CRC Press, Boca Raton
25. Lockett FJ (1972) Nonlinear viscoelastic solids. Academic, London, p 92
26. Moore DF, Geyer W (1974) A review of hysteresis theories for elastomers. Wear 30:1–34
27. Mouri H, Akutagawa K (1999) Improved tire wet traction through the use of mineral fillers. Rubber Chem Technol 72:960–968

28. Nelson BI, Dealy JM (1993) Dynamic mechanical analysis using complex waveforms. In: Collyer AA (ed) Techniques in rheological measurement. Chapman and Hall, London, pp 197–224
29. Palade LI, Verney V, Attane P (1995) Time-temperature superposition and linear viscoelasticity of polybutadienes. Macromolecules 28:7051–7057
30. Pan X-D (2004) Relationship between the dynamic softening transition and wet sliding friction of elastomer compounds. J Polym Sci B Polym Phys 42:2467–2478
31. Pan X-D, Kelley ED (2003) Enhanced apparent Payne effect in a gum vulcanizate at low temperature approaching glass transition. Polym Eng Sci 43:1512–1521
32. Pan X-D, Kelley ED, Hayes MW (2003) Bulk viscoelastic contribution to the wet-sliding friction of rubber compounds. J Polym Sci B Polym Phys 41:757–771
33. Persson BNJ (2001) Theory of rubber friction and contact mechanics. J Chem Phys 115:3840–3861
34. Powell RL, Schwarz WH (1979) Nonlinear dynamic viscoelasticity. J Rheol 23:323–352
35. Reimers MJ, Dealy JM (1996) Sliding plate rheometer studies of concentrated polystyrene solutions: large amplitude oscillatory shear of a very high molecular weight polymer in diethyl phthalate. J Rheol 40:167–186
36. Reimers MJ, Dealy JM (1998) Sliding plate rheometer studies of concentrated polystyrene solutions: nonlinear viscoelasticity and wall slip of two high molecular weight polymers in tricresyl phosphate. J Rheol 42:527–548
37. Rigney DA, Hammerberg JE (1998) Unlubricated sliding behavior of metals. MRS Bull 23:32–36
38. Rigney DA, Naylor MGS, Divakar R, Ives LK (1986) Low energy dislocation structures caused by sliding and by particle impact. Mater Sci Eng 81:409–425
39. Roberts AD (1992) A guide to estimating the friction of rubber. Rubber Chem Technol 65:673–686
40. Roland CM (1990) Dynamic mechanical behavior of filled rubber at small strains. J Rheol 34:25–34
41. Russel WB (1980) Review of the role of colloidal forces in the rheology of suspensions. J Rheol 24:287–317
42. Takino H, Nakayama R, Yamada Y, Kohjiya S, Matsuo T (1997) Viscoelastic properties of elastomers and tire wet skid resistance. Rubber Chem Technol 70:584–594
43. Wagner NJ, Bender JW (2004) The role of nanoscale forces in colloid dispersion rheology. MRS Bull 29:100–106
44. Walters K (1975) Rheometry. Chapman and Hall, London
45. Wang MJ (1999) The role of filler networking in dynamic properties of filled rubber. Rubber Chem Technol 72:430–448
46. Wang M-J, Kutsovsky Y, Zhang P, Murphy LJ, Laube S, Mahmud K (2002) New generation carbon-silica dual phase filler. Part I Characterization and application to passenger tire. Rubber Chem Technol 75:247–263
47. Wannop GL, Archard JF (1973) Elastic hysteresis and a catastrophic wear mechanism for polymers. Proc Inst Mech Eng 187:615–623
48. Wilhelm M, Maring D, Spiess HW (1998) Fourier-transform rheology. Rheol Acta 37:399–405